



HAL
open science

Universal poroelastic mechanism for hydraulic signals in biomimetic and natural branches

Jean-François Louf, Gilles Guéna, Eric Badel, Yoel Forterre

► To cite this version:

Jean-François Louf, Gilles Guéna, Eric Badel, Yoel Forterre. Universal poroelastic mechanism for hydraulic signals in biomimetic and natural branches. *Proceedings of the National Academy of Sciences of the United States of America*, 2017, 114 (42), 6 p. 10.1073/pnas.1707675114 . hal-01613620

HAL Id: hal-01613620

<https://hal.science/hal-01613620>

Submitted on 9 Oct 2017

HAL is a multi-disciplinary open access archive for the deposit and dissemination of scientific research documents, whether they are published or not. The documents may come from teaching and research institutions in France or abroad, or from public or private research centers.

L'archive ouverte pluridisciplinaire **HAL**, est destinée au dépôt et à la diffusion de documents scientifiques de niveau recherche, publiés ou non, émanant des établissements d'enseignement et de recherche français ou étrangers, des laboratoires publics ou privés.

Copyright

Universal poroelastic mechanism for hydraulic signals in biomimetic and natural branches

J.-F. Louf^a, G. Guéna^a, E. Badel^b, and Y. Forterre^{a,1}

Q:10,11 ^aAix Marseille Université, CNRS, Institut Universitaire des Systèmes Thermiques Industriels, 13013 Marseille, France; and ^bUniversité Clermont Auvergne, Institut National de la Recherche Agronomique, Protocole d'Intervention en Archéologie Funéraire, F-63000 Clermont-Ferrand, France

Edited by Howard A. Stone, Princeton University, Princeton, NJ, and approved September 11, 2017 (received for review May 9, 2017)

Plants constantly undergo external mechanical loads such as wind or touch and respond to these stimuli by acclimating their growth processes. A fascinating feature of this mechanical-induced growth response is that it can occur rapidly and at long distance from the initial site of stimulation, suggesting the existence of a fast signal that propagates across the whole plant. The nature and origin of the signal is still not understood, but it has been recently suggested that it could be purely mechanical and originate from the coupling between the local deformation of the tissues (bending) and the water pressure in the plant vascular system. Here, we address the physical origin of this hydromechanical coupling using a biomimetic strategy. We designed soft artificial branches perforated with longitudinal liquid-filled channels that mimic the basic features of natural stems and branches. In response to bending, a strong overpressure is generated in the channels that varies quadratically with the bending curvature. A model based on a mechanism analogous to the ovalization of hollow tubes enables us to predict quantitatively this nonlinear poroelastic response and identify the key physical parameters that control the generation of the pressure pulse. Further experiments conducted on natural tree branches reveal the same phenomenology. Once rescaled by the model prediction, both the biomimetic and natural branches fall on the same master curve, enlightening the universality of our poroelastic mechanism for the generation of hydraulic signals in plants.

plant biomechanics | biomimetism | long-distance signaling | poroelasticity | nonlinear beams

Q:13 **S**ince Darwin and Knight (1, 2), scientists have known that plants are able to perceive external mechanical perturbation and respond to these stimuli by modifying their growth, a process called thigmomorphogenesis (3–6). In response to mechanical stress, plants tend to decrease their elongation growth and, for plants having secondary growth like trees, increase the diameter of their organs. Over the past decades, reports have refined our understanding of thigmomorphogenesis at the biomechanical, physiological, and molecular levels (4, 7–12). A remarkable feature of this mechanically induced response is that it can be local and also nonlocal. When a shoot is bent, a sudden arrest of the elongation growth is observed far away from the perturbed area (13) within minutes (8). These experiments demonstrate that plants can carry mechanosensing information over a long distance (from centimeters to meters) very rapidly throughout the whole organ. Among the different hypotheses for this long-distance signaling [hormones transport and electrical signals (14–16)], it has long been argued that hydraulic pulses could provide a unique way for rapid communication in plants, thanks to their highly connected hydraulic network that brings water from the roots to the leaves (16–18). Propagating hydraulic waves were first mentioned by Ricca in the 1920s during his study of the sensitive plant *Mimosa pudica* (19) and later observed in different organisms in response to wounding stress, often in association with electrical waves of depolarization (20–22). Recently, Lopez et al. (23) observed that bending the stem of a whole living tree or an isolated branch seg-

ment generates a sudden overpressure that propagates rapidly in the plant vascular system. This hydraulic signal induced by a nonwounding elastic stress appears as a promising candidate for the rapid communication of the thigmomorphogenetic response. However, the physical mechanisms responsible for its generation and the parameters that govern its properties remain poorly understood. In mechanics, the hydraulic response of a porous material saturated with water, like a branch or a stem, is described by the poroelastic theory (24, 25). In this framework, the bending of a branch is expected to induce local water expulsion/suction in response to the longitudinal compression/tension strains of the plant tissues from both sides of the neutral surface of the branch. However, according to the linear beam theory, these local changes of volume should cancel each other out in average over the whole system. Therefore, it remains unclear how hydraulic signals could be generated in plants from such bending stress.

The objective of this study is to understand the origin of this hydromechanical coupling and the physical parameters that control the generation of hydraulic pulses induced by bending in plant tissues. To this end, we use a biomimetic approach (26–29) and study the hydraulic response to bending of soft artificial branches that mimic the basic structural and mechanical features of natural stems and branches. While previous theoretical and experimental works have studied the linear behavior of poroelastic beams (30–32), very few have investigated the large deformation regime of fluid-infiltrated media composed of cellular materials like wood or soft plant tissues (33). In this work, we

Significance

Plants are sessile organisms without nerves. As such, they have developed specific mechanisms to carry information rapidly throughout their body in response to mechanical stimuli. Recently, it has been suggested that the first stage of this long-distance signaling could be the propagation of hydraulic signals induced by the mechanical deformation of the plant tissue (bending), but the physical origin of this hydromechanical coupling remains a conundrum. Here, we address this issue by combining experiments on natural tree branches and soft biomimetic beams with modeling. We reveal a generic nonlinear mechanism responsible for the generation of hydraulic pulses induced by bending in poroelastic branches. Our study gives a physical basis for long-distance communication in plants based on fast hydraulic signals.

Author contributions: J.-F.L., G.G., E.B., and Y.F. designed research, performed research, analyzed data, and wrote the paper.

The authors declare no conflict of interest.

This article is a PNAS Direct Submission.

Freely available online through the PNAS open access option.

Data deposition: Data have been made available on the open-source database Zenodo Q:12 at 10.5281/zenodo.825930.

¹To whom correspondence should be addressed. Email: yoel.forterre@univ-amu.fr.

This article contains supporting information online at www.pnas.org/lookup/suppl/doi:10.1073/pnas.1707675114/-DCSupplemental.

demonstrate a generic nonlinear mechanism responsible for the generation of hydraulic pulses in both biomimetic and natural tree branches representative of wood diversity.

Results

Evidence of Hydraulic Pulses Induced by Bending in Soft Biomimetic Branches. From a mechanical perspective, tree branches and stems can be viewed in first approximation as flexible elastic beams composed of microchannels that carry water longitudinally (34, 35) (Fig. 1A). To mimic these minimal ingredients, we use polydimethylsiloxane (PDMS)-based 3D molding techniques to design soft synthetic branches (Young modulus $E \sim 0.1 - 1$ MPa, radius $R = 5$ mm, length $L = 100$ mm) perforated with parallel longitudinal microchannels (diameter $d = 500 \mu\text{m}$) with various channel numbers and array patterns (Fig. 1B and C and *Materials and Methods*). The channels are filled with a nonvolatile liquid (silicone oil) and connected together to a pressure sensor at one extremity of the beam, while the other extremity is closed (Fig. 2A). To bend the branch, we design an original setup in which one extremity of the beam is fixed and the other is moved by using a system of pivoting arms connected to a linear displacement motor (Fig. 2B and *Bending Setup for the Biomimetic Branches*). This enables us to apply a uniform curvature on the soft beam, while minimizing compressional and shearing effects within the material. The bending strain ε_B is then defined as the maximal longitudinal strain in the beam: $\varepsilon_B = \bar{C}R$ (36), where \bar{C} is the mean curvature measured by image analysis.

A typical pressure response of the synthetic branch for a bending strain ε_B of order 10% is shown in Fig. 2C. Here, the beam is initially straight, and the internal fluid pressure in the channels is equal to the atmospheric pressure $P_{\text{ref}} = P_0$ (no effect of the initial pressure is noticed as long as $|P_{\text{ref}} - P_0|$ is small compared with the beam Young's modulus E). In response to bending, a mean overpressure rises up inside the channels and reaches a steady value ΔP of the order of a few kilopascals. When the branch is brought back to its initial straight shape, the overpressure goes back to zero, showing the reversible nature of this hydraulic response. The striking observation is that the overpressure strongly increases with the bending strain, with a quadratic relationship $\Delta P \propto \varepsilon_B^2$ that is independent of the bending protocol (Fig. 2D). This nonlinearity does not come from the intrinsic material properties, since the maximal strain in our case ($\varepsilon_B \sim 0.1 - 0.2$) is far below the lin-

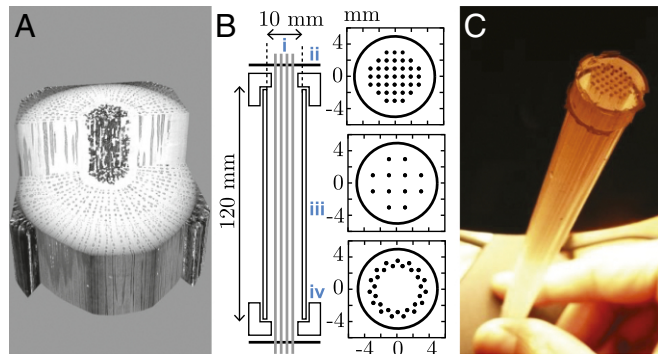


Fig. 1. Natural vs. biomimetic tree branches. (A) X-ray microtomography of a *Vitis vinifera* branch (grape vine), showing the network of longitudinal conducting vessels (dark gray). (B) Sketch of the mold used to design the synthetic branch with the different channel patterns investigated (Top, square array, $N = 37$; Middle, square array, $N = 12$; Bottom, circular array, $N = 30$): i, piano strings; ii, POM plate; iii, Plexiglas tube; iv, Plexiglas block. (C) Picture of the synthetic branch made of PDMS elastomer after removal from the mold (*Materials and Methods*).

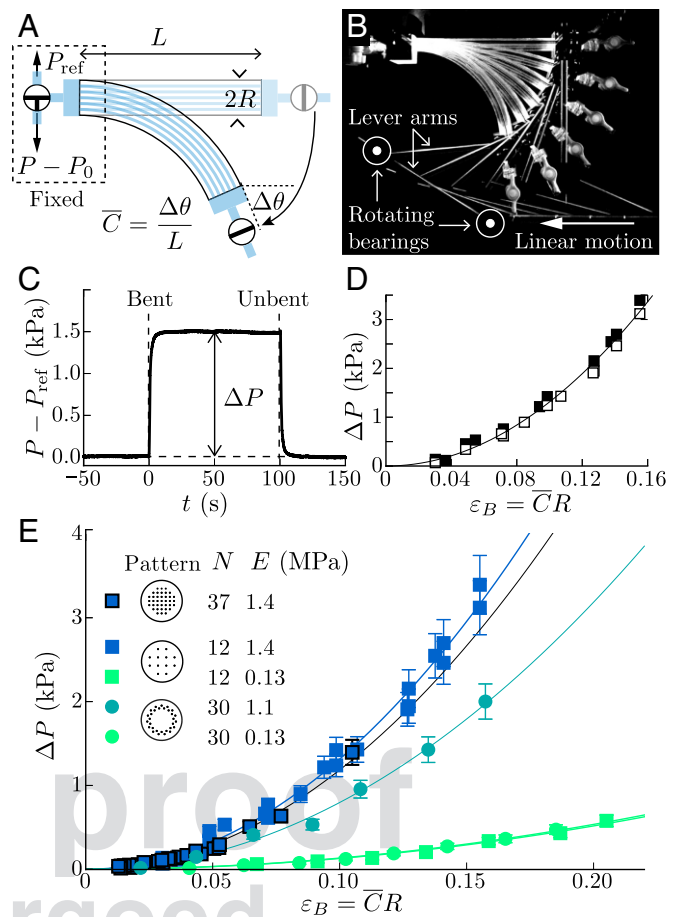


Fig. 2. Hydraulic pulse induced by bending in PDMS biomimetic branches. (A and B) Sketch (A) and picture (B) of the bending setup and pressure measurements, where $\Delta\theta$ is the variation of angle between the free extremity and the clamped extremity of the beam, \bar{C} the mean curvature of the beam, R the beam radius, P_{ref} is the initial fluid-pressure in the channels relative to the atmospheric pressure. (C) Pressure response to bending/unbending sequence in a closed system (square channel pattern, $N = 12$, $E = 1.4$ MPa, $\varepsilon_B = \bar{C}R \simeq 0.1$). (D) Steady overpressure ΔP vs. bending strain $\varepsilon_B = \bar{C}R$. Filled square, bent/unbent cycles with return to the straight state; open square, positive ramp of strain. (E) Overpressure ΔP vs. bending strain ε_B for various channel patterns, number of channels N , and PDMS Young moduli E . The solid lines in D and E are quadratic fits of the data.

ear elastic limit of the PDMS elastomer ($\varepsilon \sim 1$). Experiments with beams of different Young's modulus E and channel geometries all exhibit the quadratic relationship between the pressure and the bending strain (Fig. 2E). The response appears independent of the channels' number or distribution, but strongly increases with the beam's rigidity. This confirms that the generation of these hydraulic pulses arises from a purely elastic phenomenon.

Physical Modeling: A Nonlinear Poroelastic Coupling. Our biomimetic system therefore contains the relevant physical ingredients needed to reproduce the hydraulic pulse induced by bending recently reported in plant tissues (23). However, explaining the generation of this pulse is not straightforward. Classical linear beam theory tells us that the total volume of a symmetrical bent beam should remain constant, regardless of its elastic properties (36). This would predict a null pressure variation in a closed poroelastic beam with interconnected channels, in contradiction with observations.

249
250
251
252
253
254
255
256
257
258
259
260
261
262
263
264
265
266
267
268
269
270
271
272
273
274
275
276
277
278
279
280
281
282
283
284
285
286
287
288
289
290
291
292
293
294
295
296
297
298
299
300
301
302
303
304
305
306
307
308
309
310
311

To solve this paradox, we propose a nonlinear mechanism analogous to the ovalization of thin elastic tubes (37). When an elastic beam is bent, the longitudinal elastic strain (extension or compression) increases linearly with the distance to the neutral surface (Fig. 3 A, Left). This induces a bending elastic energy per unit volume that varies quadratically with the radius of the beam, $U_b \sim E\varepsilon_B^2 \sim EC^2R^2$, where E is the beam Young's modulus and C is the bending curvature, assumed uniform here (36). Therefore, a way for the system to lower the bending elastic energy is to squeeze its cross-section, hence decreasing the beam radius by a quantity δ in the transverse direction (Fig. 3 A, Right). The maximal bending strain then reduces to $C(R-\delta)$ and the bending energy to $U_b \sim EC^2(R-\delta)^2$. However, this transverse compression δ/R involves the cost of a positive compressive energy in the transverse direction $U_c \sim E(\delta/R)^2$. By minimizing the sum of the bending and compressive elastic energy, $\frac{d}{d\delta}(U_b + U_c) = 0$, the transverse compression is found to vary quadratically with the bending longitudinal strain: $\delta/R \sim \varepsilon_B^2$. For an elastic beam perforated with longitudinal channels, this compression is associated with a reduction of the channels' volume $\Delta V_c/V_c \sim -\delta/R$, where V_c is the total volume of the channels (38). If now the channels are filled with an incompressible liquid and closed, this reduction in volume is converted into a global rise of pore pressure $\Delta P = -B\Delta V_c/V_c$, such that:

$$\Delta P = \gamma B \varepsilon_B^2. \quad [1]$$

The coefficient B , which relates the variation of liquid volume in the channels to the change of pore pressure, is an elastic bulk modulus known as the inverse of the specific storage coefficient in the poroelastic literature (39). Dimensionally, B is proportional to the beam Young's modulus E and depends on the

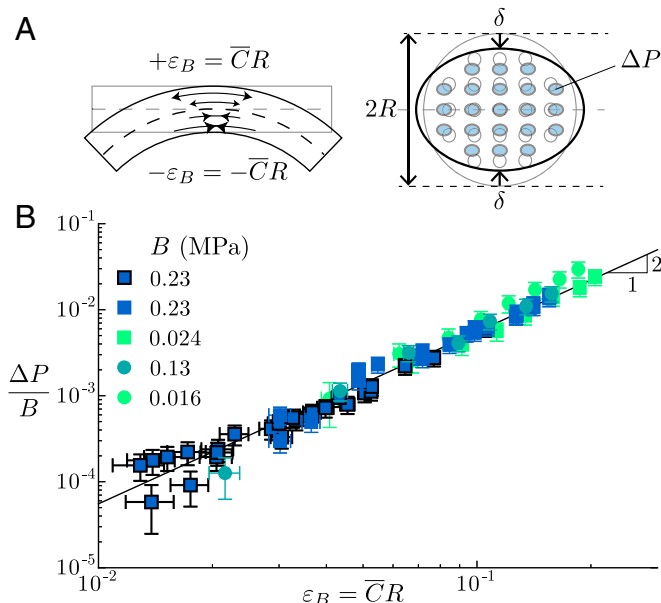


Fig. 3. Mechanism of hydraulic pulse generation and poroelastic modeling. (A) The nonlinear coupling between bending and transverse modes of deformation induces a transversal squeezing of the branch's channels $\delta/R \propto \varepsilon_B^2$ and thus an overpressure in the channels varying as $\Delta P \propto B\varepsilon_B^2$, where B is the elastic bulk modulus of the branch. (B) Overpressure ΔP normalized by the measured elastic bulk modulus B as a function of the bending deformation ε_B for all biomimetic branches studied (same symbols as in Fig. 2E). The solid line gives the best quadratic fit of the data in log-log scale: $\Delta P/B = (0.55 \pm 0.02) \times \varepsilon_B^2$ ($R^2 = 0.972$).

channels' distribution and geometry. The dimensionless factor reads $\gamma = 1/2$ in the framework of this simple energy model, which assumes a uniform transverse compression (*Energy Model for Anisotropic Beams*). A more elaborate model shows that the transverse compression is actually nonuniform and maximal at the neutral line (*Materials and Methods*, Eq. 2). As a result, γ is found to weakly depend on the channels' distribution and varies between 0.56 and 0.59 for our biomimetic beams (*Materials and Methods*, Eq. 4).

Our model therefore predicts that the bending of poroelastic beams filled with a liquid generates a global increase of the pressure that varies quadratically with the bending strain, as observed experimentally. To test Eq. 1, we independently measure the elastic bulk modulus B of the biomimetic branches (*Materials and Methods*, Eq. 2). As predicted, data for various Young's modulus and channel geometry all collapse into a single curve of slope 2 in log-log scale when overpressure is normalized by the bulk modulus B (Fig. 3B). The prefactor γ found experimentally (0.55 ± 0.02) agrees with the prediction of the model, showing the relevance of the nonlinear mechanism we propose for the generation of hydraulic pulses in the biomimetic porous branches (see *Influence of the Bending Mode on the Pressure Response* for additional comparison with the model in the case of a nonuniform curvature).

Experiments on Natural Woody Branches. To check the validity of the model in the context of plants, we conduct experiments on natural tree branches and stems (*Materials and Methods* and *Plant Materials*). Three species representative of the wood anatomy diversity are studied: a gymnosperm species (*P. sylvestris* L.), whose conducting hydraulic network is made of tiny and short conduits (tracheids) regularly distributed; a ring porous angiosperm species (*Quercus ilex* L.), where the large conducting vessels are concentrated in the earlywood zone; and a diffuse porous angiosperm species (*P. alba* \times *tremula* L. clone 717-1B4), where the conducting vessels are homogeneously distributed in the annual ring structure (40). Freshly cut, well-hydrated branches are connected at one end to a pressure sensor and sealed at the other end to create a closed vascular system (Fig. 4A and *Materials and Methods*).

First, we observe that bending generates a large increase of the water pressure in the xylem, hence confirming the first observations of Lopez et al. (23) (Fig. 4B). The overpressure is independent of the bending rate or bending history (Fig. 4C), indicating a reversible response as in the case of the biomimetic branches. Second, for all branches and species studied, we again recover a quadratic relationship between the overpressure and the bending strain (Fig. 4D), once the pressure ΔP^* and the bending strain ε_B^* are properly defined to take into account dead-volume effects and the rest natural curvature of the branches (Fig. 4; see *Extension of the Model to Beams with a Rest Curvature* and ref. 41 for the generalization of the model to naturally curved branches). The amplitude of the response for a given strain also strongly depends on the species or growing conditions, in addition to large intraspecific dispersions. By fitting the averaged data for each species and growing conditions by a quadratic law $\Delta P^* = a \times \varepsilon_B^{*2}$, we found a clear positive correlation between the amplitude factor a and the longitudinal Young's modulus $E_{||}$ of the branches (Fig. 4E). The case of *P. alba* \times *tremula* L. is especially instructive. Although all branches come from the same inbred line, the hydraulic pulse induced by bending is much higher in trees grown outside, which show much stiffer mechanical properties (red symbols in Fig. 4D and E), than trees grown indoor, which show softer properties (black symbols in Fig. 4D and E). This is a strong indication that elasticity, like in the biomimetic systems, controls the generation of the hydraulic pulse in natural branches.

311
312
313
314
315
316
317
318
319
320
321
322
323
324
325
326
327
328
329
330
APPLIED PHYSICAL SCIENCES
337
PLANT BIOLOGY
344
345
346
347
348
349
350
351
352
353
354
355
356
357
358
359
360
361
362
363
364
365
366
367
368
369
370
371
372

373
374
375
376
377
378
379
380
381
382
383
384
385
386
387
388
389
390
391
392
393
394
395
396
397
398
399
400
401
402
403
404
405
406
407
408
409
410
411
412
413
414
415
416
417
418
419
420
421
422
423
424
425
426
427
428
429
430
431
432
433
434

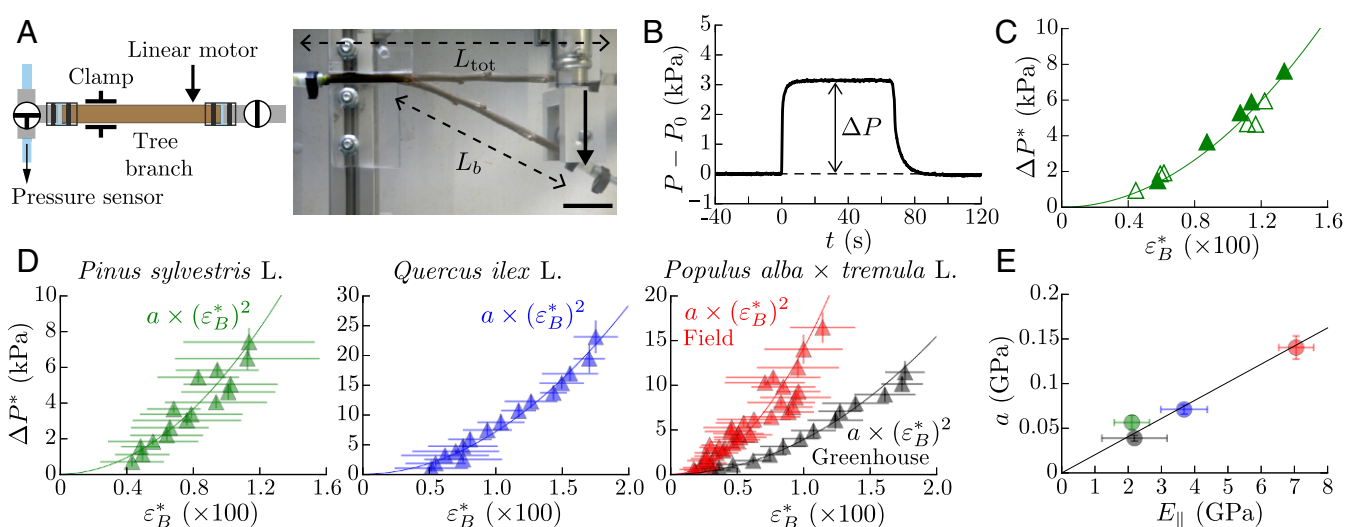


Fig. 4. Hydraulic pulse induced by bending in natural tree branches. (A) Sketch of the experimental setup, where L_{tot} is the total branch length and L_b the bent length. (Scale bar, 5 cm.) (B) Xylem water pressure measured at the fixed extremity of a pine branch (*Pinus sylvestris* L.) in response to a bent/unbent sequence. (C) Relationship between the overpressure and the bending strain for the same branch using two different bending protocols: incremental step displacement (filled symbols) and step displacement with return to the initial position after each bending (open symbols). Here, $\Delta P^* = \Delta P \times (L_{tot}/L_b)$ and $\varepsilon_B^* = \varepsilon_B(1 + \varepsilon_B^0/\varepsilon_B)^{1/2}$, where $\varepsilon_B = R(\bar{C} - \bar{C}^0)$ and $\varepsilon_B^0 = R\bar{C}^0$, with \bar{C}^0 the mean curvature of the branch at rest (*Extension of the Model to Beams with a Rest Curvature*). The solid line is a quadratic fit of the data. (D) Overpressure ΔP^* vs. bending strain ε_B^* averaged over n branches for different tree species and growing conditions (symbols) with quadratic fit $a \times \varepsilon_B^{*2}$ (solid lines). Green: *P. sylvestris* L., $n = 6$, $a = 0.056 \pm 0.008$ GPa, $R^2 = 0.91$; blue: *Q. ilex* L., $n = 5$, $a = 0.070 \pm 0.005$ GPa, $R^2 = 0.94$; red: *Populus alba* \times *tremula* L. grown in field condition, $n = 7$, $a = 0.139 \pm 0.013$ GPa, $R^2 = 0.88$; black: *P. alba* \times *tremula* L. grown in greenhouse conditions, $n = 4$, $a = 0.038 \pm 0.003$ GPa, $R^2 = 0.98$. Each symbol corresponds to a running average over five data (seven data for poplar in field conditions) with an overlap of 50%; error bars give the 5D. (E) Coefficient of the quadratic fit a as function of the longitudinal Young's modulus $E_{||}$ (same color as in D). The coefficient a is found proportional to $E_{||}$ (solid line: linear fit, $R^2 = 0.96$).

Comparison Between the Natural and Biomimetic Systems. To further investigate the similarity between the synthetic and biological branches, we gather in the Fig. 5 *Inset* the pressure response obtained in all systems as a function of the bending strain. As expected, for a given strain, the amplitude of the pressure pulse is almost three orders of magnitude larger in the natural woody branches, whose Young's moduli are of the order of a few gigapascals, than in the soft synthetic branches, whose Young's moduli are of the order of a few megapascals. More precisely, the model predicts that the relevant parameters controlling the response should be the elastic bulk modulus B of the porous beam. Such mechanical property is difficult to measure or compute in natural branches, as it would require the knowledge of both the anatomy of the conductive network and the transverse elastic properties of the wood. However, we are able to obtain reliable measurements on the poplar branches grown outdoors, giving $B = 0.37 \pm 0.08$ GPa, that is $B \simeq E_{||}/18$ (*Materials and Methods* and *Measurement of the Elastic Bulk Modulus in Woody Branches*). The bulk modulus of the other species or other growing condition is then estimated from their longitudinal Young modulus by assuming the same relationship to hold. Remarkably, when the pressure response is normalized by the value of the elastic bulk modulus of each branch, data from the biomimetic and biological systems all collapse on the same master quadratic curve over a range of 5 decades (Fig. 5). The prefactor of the law $\gamma \simeq 0.50 \pm 0.01$ is also compatible with the model prediction. This latter observation may appear surprising, as the model was built for isotropic elastic materials, while wood is highly anisotropic (orthotropic) (33, 34). A crude generalization of the energy model for orthotropic media gives: $\Delta P = B(E_{||}/4E_{\perp})(1 - \nu_{\perp})/\psi \times \varepsilon_B^2$, where E_{\perp} is the Young's modulus in the transverse direction, ν_{\perp} is an effective 2D transverse Poisson's ratio, and ψ is the volume fraction of the conductive channels (*Energy Model for Anisotropic Beams*). Our results on natural tree branches showing that $\Delta P/B \sim \varepsilon_B^2$ therefore

suggest that $(E_{||}/4E_{\perp})(1 - \nu_{\perp})/\psi \sim 1$, compatible with mechanical properties of green woods in a wide range of tree species ($E_{||} \sim 10E_{\perp}$, $\nu_{\perp} \sim 0.6$, $\psi \sim 0.5$) (33, 42). Interestingly, our prediction can also be compared with the experiments of Lopez et al. that reported hydraulic pulses in other tree species (23). In their study, they bent branches open at both ends and systematically measured the flux of water expelled during bending increments. We reanalyze their data to extract the total amount of water expelled $\Delta V_c/V_c$ as a function of the bending deformation ε_B . Although the species and experimental protocol (open vs. closed system) differ from our study, their data are found to follow the quadratic law predicted by our mechanism [*Revisiting Lopez et al. (2014)*]. The prefactor of the quadratic law is also of order one, which gives another independent measure that fulfills the relationship $(E_{||}/4E_{\perp})(1 - \nu_{\perp})/\psi \sim 1$ in woody branches.

Discussion

Hydraulic pulses induced by bending were recently put forward as a promising pathway for the rapid transmission of mechanosensing information in plants. However, how such signals could be physically generated, and how they rely on the biomechanical traits of plant tissues remained poorly understood. In this work, we address these issues using a biomimetic approach. We reveal a generic mechanism for the generation of hydraulic pressure pulses under bending, both in soft artificial branches and natural tree branches. Our mechanism relies on a nonlinear coupling between the bending and transverse mode of deformation of the beam that squeezes its cross-section, by analogy with the ovalization of thin, hollow tubes. This flattening then induces a global increase of the hydraulic pressure in the conductive channels of the branch that varies quadratically with the bending strain. Hence, unlike predictions of the linear beam theory, a nonzero hydraulic pressure pulse can be produced under bending in a poroelastic beam due to nonlinear

435
436
437
438
439
440
441
442
443
444
445
446
447
448
449
450
451
452
453
454
455
456
457
458
459
460
461
462
463
464
465
466
467
468
469
470
471
472
473
474
475
476
477
478
479
480
481
482
483
484
485
486
487
488
489
490
491
492
493
494
495
496

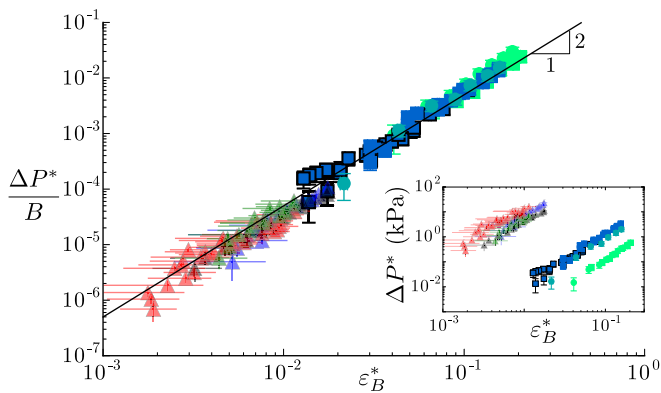


Fig. 5. Comparison between biomimetic (squares; same symbols as in Fig. 3) and natural tree branches (triangles; same symbols as in Fig. 4). The overpressure ΔP^* normalized by the elastic bulk modulus B of each branch shows a common behavior with the amplitude of the bending strain ε_B^* . The solid line represents the best quadratic fit of all data in log-log scale: $\Delta P^*/B = (0.50 \pm 0.01) \times \varepsilon_B^{*2}$ ($R^2 = 0.98$). (Inset) Overpressure vs. bending strain for all data.

geometrical effects, independent of the material properties. This finding confirms and explains the paradox previously hypothesized about the origin of hydraulic pulses induced by bending in plants (23). In an engineering context, it could also be applied to artificial devices like microfluidic pumps or soft robots to rectify pressure and fluid flow under oscillatory motion (32, 43).

The simple poroelastic model we built shows that the key parameter controlling the amplitude of the pressure response is the elastic bulk modulus of the branch, a mechanical property that mainly depends on the Young's modulus of the branch. The master curve that enlightens a unique mechanical law for artificial and natural branches is available in a wide range of material rigidities (Fig. 5), suggesting the robustness of the theoretical modeling. The few key parameters that drive the generation of the hydraulic pulse are basic patterns, which are common to all plants: the presence of a conducting hydraulic network in a rigid structure, without any further prerequisites about the other structural parameters. This suggests a universal physical phenomenon that occurs in all plants that daily experience the mechanical loads of the wind (44).

Our study therefore gives a physical basis for long-distance communication in plants based on hydraulic signals. However, for these pressure pulses to function as information carriers, they must fulfill two main conditions: (i) they should transfer rapidly information from the places that experience the mechanical stimuli to the apical zones that sense the signal; and (ii) they should be perceived and converted to a relevant physiological response (thigmomorphogenetic growth response).

According to our study, a bending strain of few percent caused by wind sway (44) generates a hydraulic pressure pulse of amplitude 0.01–0.1 MPa without change of conductivity (the squeezing of the cross-section is of order $\sim 10^{-4}$). This pressure pulse first propagates ballistically at the speed of the compressive elastic waves $c = \sqrt{B/\rho} \simeq 500 \text{ m s}^{-1}$ (ρ is the water density) (45), then spreads with a diffusive dynamics when viscous effects prevail over inertia. This cross-over between the ballistic and diffusive regime naturally defines an effective range L_b of propagation without damping when the inertial timescale $\tau_i \sim L_b/c$ becomes equal to the poroelastic timescale $\tau_p \sim L_b^2/D$ (25), where $D \sim d^2 B/\eta$ is a longitudinal diffusion coefficient related to the channels diameter d , the channel elasticity B , and the water viscosity η . Typical values for woody tissues give $L_b \sim D/c \sim 1 \text{ m}$ ($d \sim 50 \text{ }\mu\text{m}$, $B \sim 0.3 \text{ GPa}$, $\eta \sim 1 \text{ mPa s}$).

Beyond this length, the hydraulic signal still propagates rapidly, but with a diffusive dynamics (the effective speed of the diffusion front D/L is about 50 m s^{-1} for a traveling distance $L = 10 \text{ m}$).

Even though hydraulic pulses spread rapidly throughout the conductive network, whether they are perceived or not as a signal is still an open question. Typical pressure pulses induced by bending are one order of magnitude smaller in amplitude than the slow daily variation of the (negative) water pressure in the conductive network of transpiring plants (35), but their frequency is much higher (typically a few hertz). This separation of amplitude and time scales is found in most biological sensory systems (46). How this overpressure may be sensed in the apical part is still under debate, but recent works suggest that mechanosensing channels could be involved in this transduction process (11, 12), opening the pathway for ion fluxes that generate local electrical signals and molecular responses (16). Future works are needed to address these issues and establish whether thigmomorphogenesis in plants do rely on this peculiar mode of signaling: hydraulics.

Materials and Methods

Experiments on Biomimetic Branches. Synthetic branches are made in PDMS with the Sylgard 184 Silicone Elastomer Kit using either 10% or 4% (wt) cross-linker (degassed for 30 min). The liquid PDMS is injected in a negative 3D mold made of a poly(methyl methacrylate) (PMMA) tube (length: $Q:14$ $L = 10 \text{ cm}$, inner diameter $D = 1 \text{ cm}$) containing piano strings (diameter $d = 500 \text{ }\mu\text{m}$) fixed at both extremities in a pattern of holes drilled in a POM plate. Once cured (1 wk at $60 \text{ }^\circ\text{C}$), the solid PDMS beam is removed: $Q:15$ from the mold and fitted into two perforated PMMA blocks. The channels are then filled with a viscous silicone oil (viscosity $1 \text{ Pa}\cdot\text{s}$) and connected together to a differential pressure sensor. The Young's modulus E of the beam's matrix is determined from plain slender rods of PDMS by using a tensile testing device in the linear regime of deformation ($<25\%$). The elastic bulk modulus B of the synthetic branches is determined by injecting a given amount of liquid inside the channels with a microsyringe and measuring the corresponding increase of liquid pressure. The beams are bent either manually or by using an automated bending device (see [Bending Setup for the Biomimetic Branches](#) for details). The mean curvature of the beam is measured from the difference of the angle of the beam's profile at both extremities.

Experiments with Plant Materials. All experiments are conducted between May and September on well-watered trees (see [Plant Materials](#) for details on the species and growing conditions). Buds and leaves are removed a few days before collecting the materials, and the scars are glued to avoid leaks during measurements. The cutting of branches and stems is done following the method described in ref. 47 to avoid any air contamination in the conducting system. The branches are then plugged to the experimental setup and flushed for several hours with degassed water to fill the conductive hydraulic network. During the bending, the branches are either in air or immersed in water to avoid evaporation. The determination of the longitudinal Young's modulus E_{\parallel} of the branches is done after each experiment by using a standard four-point bending test. The determination of the elastic bulk modulus B of the channels is done by applying pressure increments ΔP to the water-saturated xylem of the branch ([Measurement of the Elastic Bulk Modulus in Woody Branches](#)).

Refined Model. In the main text, the quadratic relationship [1] between the hydraulic overpressure ΔP and the bending strain ε_B is obtained from simple scaling arguments, assuming a uniform transverse strain $\varepsilon_{\perp} \sim \delta/R$ in the cross-section of the beam. Here, the prefactor γ of the scaling law is computed by taking into account the spatial variation of the transverse strain. For a cylindrical elastic beam of radius R , bent with a uniform curvature C , the balance of the bending longitudinal stress implies the existence of a compressive stress in the transverse direction due to the finite curvature of the beam. This second-order effect in the slender beam parameter RC is responsible for the ovalization of the cross-section and gives rise to a parabolic transverse strain field given by ref. 48:

$$\varepsilon_{\perp}(z) = \frac{1}{3} \left[1 - \left(\frac{z}{R} \right)^2 \right] \times \varepsilon_B^2, \quad [2]$$

where $\varepsilon_B = RC$ and z is the height from the neutral line. To compute the liquid overpressure ΔP_i generated by this transverse compression field in the i^{th} channel, a mean field approach is used in the limit of low channel density (low porosity). Each channel at height z_i filled with an incompressible fluid is assumed to deform as if it was isolated in an effective infinite elastic medium and subjected to an external uniform compression field $\varepsilon_{\perp}(z_i)$. By using the superposition principle, the relative change of volume Δv_i of each channel is then given by the sum of the volume variation induced by the transverse compression strain $\varepsilon_{\perp}(z_i)$ and by the overpressure ΔP_i (see ref. 36, chapter 13, problem 5, and chapter 7, problem 4); that is:

$$\frac{\Delta v_i}{v_i} = -2 \times \varepsilon_{\perp}(z_i) + \frac{\Delta P_i}{B_i}, \quad [3]$$

where v_i is the channel volume and B_i is the channel bulk modulus as defined in the main text. In a closed system, the incompressibility of the liquid implies $\sum_i \Delta v_i = 0$. Moreover, in natural branches and in our exper-

iments, the channels are always interconnected hydraulically, so the overpressure is uniform ($\Delta P_i = \Delta P$). Therefore, substituting Eq. 2 in Eq. 3 and summing over all channels for identical channels ($B_i = B$ and $v_i = v$) gives Eq. 1 with:

$$\gamma = \frac{2}{3N} \sum_{i=1}^N \left[1 - \left(\frac{z_i}{R} \right)^2 \right], \quad [4]$$

where N is the number of channels.

ACKNOWLEDGMENTS. We thank Brigitte Girard and Pierre Conchon for their help with the wood microslices preparations on tree branches. This work was supported by Agence Nationale de la Recherche Jeunes Chercheurs et Jeunes Chercheurs ARTIS Grant ANR-13-JS09-0011-01, Labex MEC Grant ANR-10-LABX-0092, the A*MIDEX Project (ANR-11-IDEX-0001-02) funded by the French government program Investissements d'avenir, and the European Research Council under European Union Horizon 2020 Research and Innovation Program Grant 647384.

1. Darwin C, Darwin F (1880) *The Power of Movement in Plants* (Murray, London).
2. Knight TA (1803) Account of some experiments on the descent of the sap in trees. *Phil Trans Roy Soc Lond* 93:277–289.
3. Jaffe MJ, Leopold AC, Staples RC (2002) Thigmo responses in plants and fungi. *Am J Bot* 89:375–382.
4. Braam J (2005) In touch: Plant responses to mechanical stimuli. *New Phytol* 165:373–389.
5. Telewski FW (2006) A unified hypothesis of mechanoperception in plants. *Am J Bot* 93:1466–1476.
6. Coutand C (2010) Mechanosensing and thigmomorphogenesis, a physiological and biomechanical point of view. *Plant Sci* 179:168–182.
7. Knight MR, Smith SM, Trewavas AJ (1992) Wind-induced plant motion immediately increases cytosolic calcium. *Proc Natl Acad Sci USA* 89:4967–4971.
8. Coutand C, Julien JL, Mouliia B, Mauget JC, Guitard D (2000) Biomechanical study of the effect of a controlled bending on tomato stem elongation: Global mechanical analysis. *J Exp Bot* 51:1813–1824.
9. Kern KA, Ewers FW, Telewski FW, Koehler L (2005) Mechanical perturbation affects conductivity, mechanical properties and aboveground biomass of hybrid poplars. *Tree Physiol* 25:1243–1251.
10. Coutand C, et al. (2009) Strain mechanosensing quantitatively controls diameter growth and PtZFP2 gene expression in poplar. *Plant Physiol* 151:223–232.
11. Monshausen GB, Haswell ES (2013) A force of nature: Molecular mechanisms of mechanoperception in plants. *J Exp Bot* 64:4663–4680.
12. Peyronnet R, Tran D, Girault T, Frachisse JM (2014) Mechanosensitive channels: Feeling tension in a world under pressure. *Front Plant Sci* 5:558.
13. Patterson MR (1992) Role of mechanical loading in growth of sunflower (*Helianthus annuus*) seedlings. *J Exp Bot* 43:933–939.
14. Mousavi SAR, Chauvin A, Pascaud F, Kellenberger S, Farmer EE (2013) GLUTAMATE RECEPTOR-LIKE genes mediate leaf-to-leaf wound signalling. *Nature* 500:422–426.
15. Hedrich R, Salvador-Recatalá V, Dreyer I (2016) Electrical wiring and long-distance plant communication. *Trends Plant Sci* 21:376–387.
16. Choi WG, Hilleary R, Swanson SJ, Kim SH, Gilroy S (2016) Rapid, long-distance electrical and calcium signaling in plants. *Annu Rev Plant Biol* 67:287–307.
17. Christmann A, Grill E, Huang J (2013) Hydraulic signals in long-distance signaling. *Curr Opin Plant Biol* 16:293–300.
18. Farmer EE, Gasperini D, Acosta IF (2014) The squeeze cell hypothesis for the activation of jasmonate synthesis in response to wounding. *New Phytol* 204:282–288.
19. Ricca U (1926) Transmission of stimuli in plants. *Nature* 117:654–655.
20. Malone M (1993) Hydraulic signals. *Phil Trans Roy Soc B Biol Sci* 341:33–39.
21. Stahlberg R, Cosgrove D (1995) Comparison of electric and growth responses to excision in cucumber and pea seedlings. ii. Long-distance effects are caused by the release of xylem pressure. *Plant Cell Environ* 18:33–41.
22. Stankovic B, Zawadzki T, Davies E (1997) Characterization of the variation potential in sunflower. *Plant Physiol* 115:1083–1088.
23. Lopez R, et al. (2014) Tree shoot bending generates hydraulic pressure pulses: A new long-distance signal? *J Exp Bot* 65:1997–2008.
24. Biot MA (1941) General theory of three-dimensional consolidation. *J Appl Phys* 12:155–164.
25. Dumais J, Forterre Y (2012) “Vegetable dynamics”: The role of water in plant movements. *Annu Rev Fluid Mech* 44:453–478.
26. Noblin X, et al. (2008) Optimal vein density in artificial and real leaves. *Proc Natl Acad Sci USA* 105:9140–9144.
27. Wheeler T, Stroock A (2008) The transpiration of water at negative pressures in a synthetic tree. *Nature* 455:208–212.
28. Vincent O, Marmottant P, Gonzalez-Avila S, Ando K, Ohl CD (2014) The fast dynamics of cavitation bubbles within water confined in elastic solids. *Soft Matter* 10:1455–1461.
29. Zwieniecki MA, Haaning KS, Boyce CK, Jensen KH (2016) Stomatal design principles in synthetic and real leaves. *J R Soc Interface* 13:20160535.
30. Skotheim JM, Mahadevan L (2004) Dynamics of poroelastic filaments. *Proc R Soc A Math Phys Eng Sci* 460:1995–2020.
31. Scherer GW (1996) Bending a gel rod with an impermeable surface. *J Non Cryst Solids* 204:73–77.
32. Holmes DP, Tavakol B, Froehlicher G, Stone HA (2013) Control and manipulation of microfluidic flow via elastic deformations. *Soft Matter* 9:7049–7053.
33. Gibson LJ, Ashby MF (1999) *Cellular Solids, Structure and Properties* (Cambridge Univ Press, Cambridge, UK).
34. Niklas K (1992) *Plant Biomechanics: An Engineering Approach to Plant Form and Function* (Univ of Chicago Press, Chicago).
35. Tyree MT, Zimmermann MH (2002) *Xylem Structure and the Ascent of Sap* (Springer, New York).
36. Landau LD, Lifshitz EM (1986) *Theory of Elasticity* (Elsevier, New York).
37. Brazier LG (1927) On the flexure of thin cylindrical shells and other “Thin” sections. *Proc R Soc A Math Phys Eng Sci* 116:104–114.
38. Day AR, Snyder KA, Garboczi EJ, Thorpe MF (1992) The elastic moduli of a sheet containing circular holes. *J Mech Phys Solids* 40:1031–1051.
39. Wang H (2000) *Theory of Linear Poroelasticity with Applications to Geomechanics and Hydrogeology* (Princeton Univ Press, Princeton).
40. Crivellaro A, Schweingruber FH (2015) *Stem Anatomical Features of Dicotyledons* (Kessel, Remagen, Germany).
41. Clark R, Reissner E (1951) Bending of curved tubes. *Adv Appl Mech* 2:93–122.
42. Green DW, Winandy JE, Kretschmann DE (1999) Mechanical properties of wood. *Q:20 Wood Handbook: Wood as an Engineering Material* (Forest Products Laboratory, Madison, WI.), pp 4-1–4-45.
43. Shepherd RF, et al. (2011) Multigait soft robot. *Proc Natl Acad Sci USA* 108:20400–20403.
44. De Langre E (2008) Effects of wind on plants. *Annu Rev Fluid Mech* 40:141–168.
45. Knipfler T, Steudle E (2008) Root hydraulic conductivity measured by pressure clamp is substantially affected by internal unstirred layers. *J Exp Bot* 59:2071–2084.
46. Smith CUM (2008) *Biology of Sensory Systems* (John Wiley & Sons, New York).
47. Wheeler JK, Huggett BA, Tofte AN, Rockwell FE, Holbrook NM (2013) Cutting xylem under tension or supersaturated with gas can generate PLC and the appearance of rapid recovery from embolism. *Plant Cell Environ* 36:1938–1949.
48. Ennos A, van Casteren A (2010) Transverse stresses and modes of failure in tree branches and other beams. *Proc Biol Sci* 277:1253–1258.

AUTHOR QUERIES

AUTHOR PLEASE ANSWER ALL QUERIES

1

- Q: 1_Please contact PNAS_Specialist.djs@sheridan.com if you have questions about the editorial changes, this list of queries, or the figures in your article. Please include your manuscript number in the subject line of all email correspondence; your manuscript number is 201707675.
- Q: 2_Please (i) review the author affiliation and footnote symbols carefully, (ii) check the order of the author names, and (iii) check the spelling of all author names, initials, and affiliations. Please check with your coauthors about how they want their names and affiliations to appear. To confirm that the author and affiliation lines are correct, add the comment “OK” next to the author line. This is your final opportunity to correct any errors prior to publication. Misspelled names or missing initials will affect an author’s searchability. Once a manuscript publishes online, any corrections (if approved) will require publishing an erratum; there is a processing fee for approved erratum.
- Q: 3_Please review and confirm your approval of the short title: Hydraulic signals in biomimetic branches. If you wish to make further changes, please adhere to the 50-character limit. (NOTE: The short title is used only for the mobile app and the RSS feed.)
- Q: 4_Please review the information in the author contribution footnote carefully. Please make sure that the information is correct and that the correct author initials are listed. Note that the order of author initials matches the order of the author line per journal style. You may add contributions to the list in the footnote; however, funding should not be an author’s only contribution to the work.
- Q: 5_Please confirm that the author names appear as they should in the paper. In the cover sheet, authors have first names rather than just initials listed.
- Q: 6_You have chosen the PNAS open access option for your paper and have agreed to pay additional open access fees. Please confirm that this is correct. If this is incorrect, and you decline to pay open access fees, please note this in the margin.
- Q: 7_Please verify that all callouts for supporting information (SI) in text are correct. Note, however, that the hyperlinks for SI callouts will not work until the article is published online. In addition, SI that is not composed in the main SI PDF (appendices, datasets, movies, and “Other Supporting Information Files”) have not been changed from your originally submitted file and so are not included in this set of proofs. The proofs for any composed portion of your SI are included in this proof as subsequent pages following the last page of the main text. If you did not receive the proofs for your SI, please contact PNAS_Specialist.djs@sheridan.com.
- Q: 8_Please check the order of your keywords and approve or reorder them as necessary. Note that PNAS allows up to five keywords; please do not add new keywords unless you wish to replace others.
- Q: 9_ Per PNAS style, certain compound terms are hyphenated when used as adjectives and unhyphenated when used as nouns. This style has been applied consistently throughout where (and if) applicable.
- Q: 10_Please confirm that abbreviations were spelled out correctly in the affiliations.
- Q: 11_Please confirm that the postal code added to the affiliations is correct.

AUTHOR QUERIES

AUTHOR PLEASE ANSWER ALL QUERIES

2

- Q: 12_Please indicate whether the data have been deposited in PDB or another publicly accessible database before your page proofs are returned. It is PNAS policy that the data be deposited BEFORE the paper can be published.
- Q: 13_PNAS prefers that any and all numbered composed pieces of Supporting Information be cited in the article's main text so that they may be integrated into the full text (HTML) presentation of the article online. The following components are not cited in your article: Figs. S1, S2, S3, S4, and S5. Please cite these components in numerical order in the main text if possible.
- Q: 14_Please confirm that PMMA was spelled out correctly.
- Q: 15_Please spell out POM if possible.
- Q: 16_Please clarify which section of the text (such as Results or Discussion) is meant by "In the main text."
- Q: 17_Please clarify which section of the text (such as Results or Discussion) is meant by "as defined in the main text."
- Q: 18_Please confirm that ANR and JCJC were spelled out correctly.
- Q: 19_Please spell out ARTIS, MEC, and A*MIDEX if possible.
- Q: 20_For ref. 42, please confirm publisher and location.



Supporting Information

Louf et al. 10.1073/pnas.1707675114

Bending Setup for the Biomimetic Branches

The automatic bending setup for the biomimetic branches consists of a linear motor and two lever arms connected by two rotating bearings (Fig. S1 *A* and *B*). This configuration is chosen to explore a wide range of bending deformation and impose a uniform bending along the beam, while minimizing shearing effects. Two deviations from pure bending nevertheless arise with this setup. First, there exists a mean compression stress in the longitudinal direction of magnitude $N/A = M/(AL_B)$ (M is the bending torque, L_B is the length of the lever arm, and $A = \pi R^2$ is the section of the beam), which adds to the bending stress $\sigma_{\parallel}(z) = (M/I) \times z$ ($I = \pi R^2/4$). As a consequence, the neutral surface is shifted by a distance $z_N = R^2/(4L_B)$. Second, in addition to the constant torque M , there exists a torque induced by the transverse effort T that varies linearly along the beam and whose maximal magnitude is $M_T = TL = N \tan \theta L = M \tan \theta (L/L_B)$, where L is the length of the beam. In practice, both effects are minimized by maximizing the length of the lever arm L_B (typically $z_N/R \sim 1/20$ and $M_T/M < 1/5$). Direct measurements of the curvature profile show that the curvature is approximately uniform along the beam for a wide range of imposed curvature (Fig. S1 *C* and *D*).

Energy Model for Anisotropic Beams

The energy model given in the main text can be easily extended to anisotropic beams characterized by a longitudinal Young's modulus E_{\parallel} different from the transverse Young's modulus E_{\perp} , which is a first approximation of the orthotropic behavior of natural branches. The bending elastic energy per unit volume of the ovalized beam then writes $U_b = (1/8)E_{\parallel}(R - \delta)^2 C^2$ (with the prefactor corresponding to a circular cross-section; ref. 36), while the compressive elastic energy per unit volume writes $U_c = (1/2)E_{\perp}(\delta/R)^2$. The minimization of the total bending energy thus gives: $\delta = (E_{\parallel}/4E_{\perp})R^2 C^2 = (E_{\parallel}/4E_{\perp})\varepsilon_B^2$. The change of area of the beam's cross-section ΔA associated to this transverse compression is given by: $\Delta A/A = -(1 - \nu_{\perp})(\delta/R)$, where A is the beam cross-section and ν_{\perp} is an effective 2D Poisson's ratio in the transverse direction (38). Since by definition $A_c = \psi A$ and assuming $\Delta A \approx \Delta A_c$ gives $\Delta A/A \approx \psi \Delta A_c/A_c \approx \psi \Delta V_c/V_c$. Using the definition of the bulk modulus and the previous expressions yields:

$$\Delta P = \gamma B \varepsilon_B^2 \quad \text{with} \quad \gamma = \frac{E_{\parallel}}{4E_{\perp}} \frac{1 - \nu_{\perp}}{\psi} \varepsilon_B^2. \quad [\text{S1}]$$

For isotropic media ($E_{\parallel} = E_{\perp}$), it can be shown that $(1 - \nu_{\perp})/\psi = 2$ in the dilute channel limit with an incompressible elastic matrix (38), yielding $\gamma = 1/2$.

Influence of the Bending Mode on the Pressure Response

In the main text, experiments on the biomimetic branches are done by applying a uniform curvature C on the beam. We perform complementary experiments using a cantilever geometry, where the curvature varies linearly along the beam: $C(x) = 2\bar{C}[1 - (x/L)]$ (Fig. S2, red inset). Assuming that the quadratic relation between the change of channels' volume and the bending deformation holds locally, the model predicts that the pressure response is:

$$\begin{aligned} \Delta P &= B \frac{|\Delta V_c|}{V_c} = \frac{B}{L} \int_0^L \gamma C(x)^2 R^2 dx \\ &= \frac{4}{3} \gamma B (R\bar{C})^2 = \frac{4}{3} \gamma B \varepsilon_B^2. \end{aligned} \quad [\text{S2}]$$

For a given mean curvature, the coefficient of the scaling law is therefore amplified by a factor 4/3 for a linear distribution of curvature compared with the case of a uniform curvature. Such amplification is recovered in the experiments, with an amplification ratio (1.55 ± 0.15) slightly larger than the predicted one (Fig. S2).

Extension of the Model to Beams with a Rest Curvature

The quadratic dependence of the poroelastic response observed with the synthetic branches naturally reflects the $C \rightarrow -C$ symmetry of these straight beams. For a beam with a small rest curvature C_0 , which is the case of most natural tree branches, this symmetry is broken, and one expects a linear pressure response as long as the imposed curvature increment $dC = C - C_0$ is small compared with C_0 . To extend the model to such initially curved beams, we follow the geometrical approach proposed by ref. 41 for thin curved tubes. A beam of radius R with a rest curvature $C_0 = 1/R_0$ is brought to the curvature $C = C_0 + dC$. Due to the ovalization phenomenon, the cross-section is squeezed by a quantity δ in the curvature plane (Fig. S3). Let \mathcal{L}_0 be the length of the fiber located at distance R from the neutral surface in the rest state and \mathcal{L} its length after the increment of curvature, which brings the fiber at $R - \delta$. Geometrical relations implies $\mathcal{L}_0 = \mathcal{L}_{00}(1 + C_0 R)$ and $\mathcal{L} = \mathcal{L}_{00}(1 + C(R - \delta))$, where \mathcal{L}_{00} is the length of the neutral surface equal in both states by definition. The corresponding longitudinal deformation associated with bending is therefore: $\varepsilon_{\parallel} = (\mathcal{L} - \mathcal{L}_0)/\mathcal{L}_0 \approx -C_0 \delta + dC \cdot (R - \delta)$ in the limit of small rest curvature ($RC_0 \ll 1$); that is, $\varepsilon_{\parallel} = -\varepsilon_0 \varepsilon_{\perp} + \varepsilon_B(1 - \varepsilon_{\perp})$, where $\varepsilon_B \equiv (C - C_0)R$, $\varepsilon_B^0 \equiv C_0 R$ and $\varepsilon_{\perp} \equiv \delta/R$, as defined in the main text. By minimizing the sum of the elastic bending energy $U_b \sim E \varepsilon_{\parallel}^2$ and compressive energy in the transverse direction $U_c \sim E \varepsilon_{\perp}^2$ (per unit volume) with respect to ε_{\perp} , one obtains:

$$\varepsilon_{\perp} \sim \varepsilon_B(\varepsilon_0 + \varepsilon_B). \quad [\text{S3}]$$

Therefore, for a poroelastic beam with a rest curvature, the rise in pressure induced by bending is expected to vary as:

$$\Delta P \sim \gamma B \varepsilon_B^{*2} \quad \text{where} \quad \varepsilon_B^* = \varepsilon_B \left(1 + \frac{\varepsilon_B^0}{\varepsilon_B}\right)^{1/2}. \quad [\text{S4}]$$

When $\varepsilon_B^0 \gg \varepsilon_B$ (large rest curvature and/or small deformation), the poroelastic response is linear and given by $\Delta P = \gamma \varepsilon_0 \varepsilon_B$. By contrast, when $\varepsilon_B^0 \ll \varepsilon_B$ (small rest curvature and/or large deformation), one recovers the quadratic relationship with the bending deformation of straight beams: $\Delta P = \gamma B \varepsilon_B^2$.

Plant Materials

Branches of *P. sylvestris* with diameters ranging from 0.8 to 1.6 cm and length from 20 to 36 cm are collected on mature trees in the wild at the Puy de la Vache, Puy-de-Dôme, France [N 45.4°, E 2.6°]. Branches of *Q. ilex* with diameters ranging from 0.6 to 1.1 cm and lengths from 18 to 21 cm are collected from cultivated trees grown in a greenhouse. Experiments on poplars are done on hybrids (*P. tremula* × *P. alba* L., clone 717-1B4) (see ref. 10 for details). One set of experiments is done on 6-mo-old stems grown in a greenhouse, with diameters ranging from 0.5 to 1.2 cm and lengths from 11 to 20 cm. A second set of experiments is done on 1- to 2-y-old branches with diameters ranging from 0.9 to 1.1 cm and lengths from 25 to 33 cm, taken from 4-y old poplars grown in an outdoor orchard at the Institut National de

125 q:3 la Recherche Agronomique site of Crouël, Clermont-Ferrand,
126 France [N 45.8°, E 3.2°].

127 Measurement of the Elastic Bulk Modulus in Woody Branches

128 Pressure increments ΔP are applied to the water-saturated
129 xylem of the branch by using a compressed air bottle connected
130 to the liquid (Fig. S4A). The relative variation of volume of
131 the branch induced by the change of pressure is then measured
132 by using a strain gauge glued in the transverse direction:
133 $\Delta V/V = 2\Delta R/R$, where $\Delta R/R$ is the relative variation of the
134 branch radius and V the total volume of the branch. The change
135 of length of the branch $\Delta L/L$ is neglected in the computation
136 of the variation of $\Delta V/V$, as the longitudinal strain is found to
137 be 10 times smaller than the radial deformation (consistent with
138 the fact that the longitudinal Young's modulus of wood is much
139 larger than the transverse Young's modulus). From this measure-
140 ments, we obtain the macroscopic bulk modulus of the branch,
141 defined by: $B_{\text{macro}} \equiv V(\Delta P/\Delta V)$. Assuming that the change of
142 the branch volume is equal to the change of volume of the con-
143 ductive channels, $\Delta V = \Delta V_c$ (the compressibility of the cell wall
144 is negligible compared with the compressibility of the channels),
145 and denoting ψ the liquid fraction of the channels, $\psi = V_c/V$,
146 the channel bulk modulus can be obtained from the macroscopic
147 bulk modulus as: $B = \psi B_{\text{macro}}$. To measure the liquid fraction
148 of the channel, thin cytological (16 μm) transverse sections
149 of poplar branches (without bark) are stained by using safranin and
150 visualized with a microscope (Fig. S4B). Images are then bina-

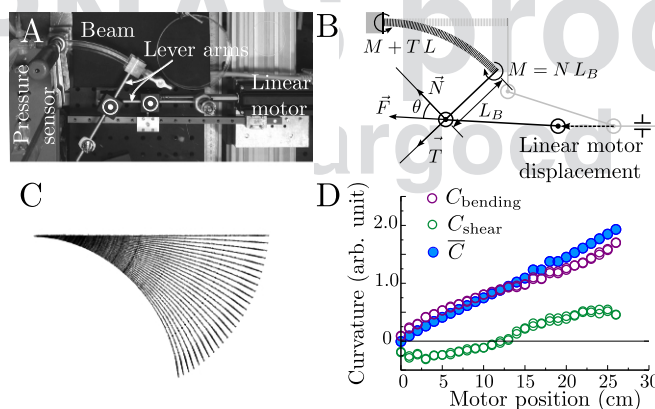
187 rized and analyzed by using the software ImageJ to compute the
188 surface fraction of voids $\psi = 0.36 \pm 0.05$.

189 Revisiting Lopez et al. (2014)

190 In their study (23), Lopez et al. reported a linear correlation
191 between the volume of expelled water (called pulse volume in the
192 paper) and the bending deformation ε_B , in a series of four-point
193 bending experiments on open branches from five tree species
194 (table 1 and figure 8 of ref. 23). Such linear relationship may
195 appear in contradiction with the quadratic law predicted by our
196 mechanism. However, the pulse volume in their study corre-
197 sponds to the volume $\delta V_c(\varepsilon_B)$ expelled during the *increment*
198 of deformation $\delta\varepsilon_B$, not during the entire deformation from the ini-
199 tial rest state. From their raw data, we compute the total amount
200 of water expelled at the deformation ε_B as:

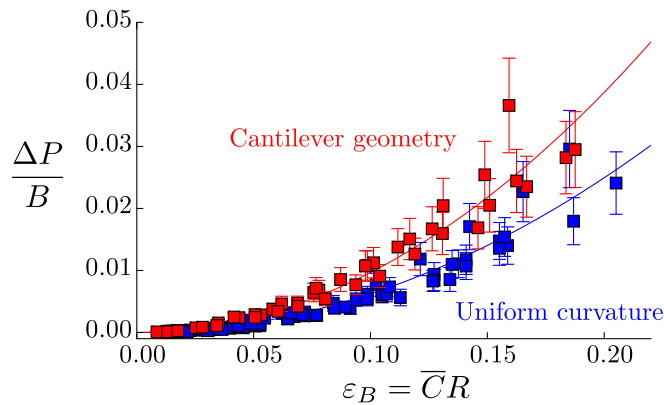
$$201 \Delta V_c = \sum_{\varepsilon=0}^{\varepsilon=\varepsilon_B} \delta V_c(\varepsilon). \quad [S5] \quad 202$$

203 The total volume of water channels V_c is then estimated as the
204 volume of the bent lumen reported in their study for each species
205 (the volume of the lumen is equal to the volume of the branch
206 minus the total volume of the cell wall). With this proper repre-
207 sentation, data from Lopez et al. (23) reveal the quadratic rela-
208 tionship $\Delta V_c/V_c = \gamma\varepsilon_B^2$ predicted by the model (Fig. S5), with a
209 prefactor γ larger but of the same order of magnitude as in our
210 experiments (Fig. S4 *Inset*).
211

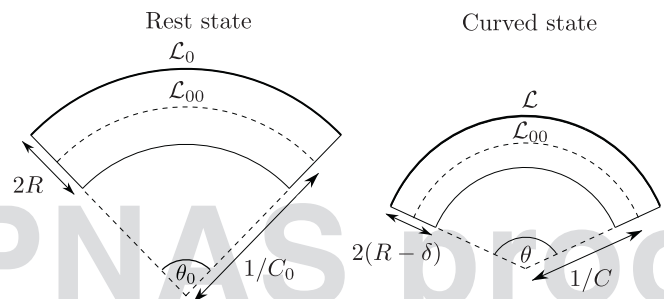


151
152
153
154
155
156
157
158
159
160
161
162
163
164
165
166
167
168
169
170
171
172
173
174
175
176
177
178
179
180
181
182
183
184
185
186
187
188
189
190
191
192
193
194
195
196
197
198
199
200
201
202
203
204
205
206
207
208
209
210
211
212
213
214
215
216
217
218
219
220
221
222
223
224
225
226
227
228
229
230
231
232
233
234
235
236
237
238
239
240
241
242
243
244
245
246
247
248
249
250
251
252
253
254
255
256
257
258
259
260
261
262
263
264
265
266
267
268
269
270
271
272
273
274
275
276
277
278
279
280
281
282
283
284
285
286
287
288
289
290
291
292
293
294
295
296
297
298
299
300
301
302
303
304
305
306
307
308
309
310
311
312
313
314
315
316
317
318
319
320
321
322
323
324
325
326
327
328
329
330
331
332
333
334
335
336
337
338
339
340
341
342
343
344
345
346
347
348
349
350
351
352
353
354
355
356
357
358
359
360
361
362
363
364
365
366
367
368
369
370
371
372
373
374
375
376
377
378
379
380
381
382
383
384
385
386
387
388
389
390
391
392
393
394
395
396
397
398
399
400
401
402
403
404
405
406
407
408
409
410
411
412
413
414
415
416
417
418
419
420
421
422
423
424
425
426
427
428
429
430
431
432
433
434
435
436
437
438
439
440
441
442
443
444
445
446
447
448
449
450
451
452
453
454
455
456
457
458
459
460
461
462
463
464
465
466
467
468
469
470
471
472
473
474
475
476
477
478
479
480
481
482
483
484
485
486
487
488
489
490
491
492
493
494
495
496
497
498
499
500

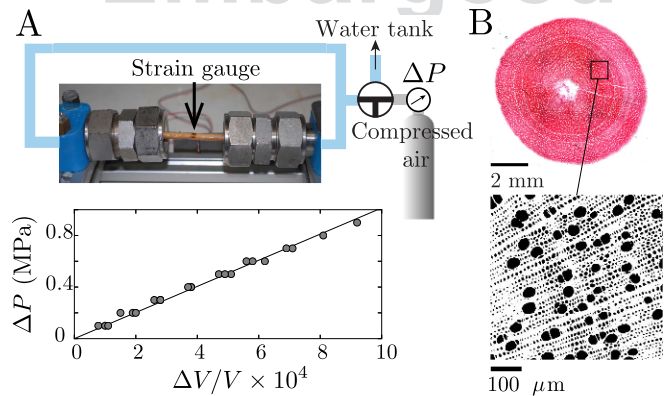
Fig. S1. (A) Top view of the bending setup, including a linear motor, lever arms, and rotating bearings. (B) Force balance on the bent beam. Once the displacement is imposed, the beam is subject to a force F which creates a bending moment $M = NL_B$, a compression force N , and a tangential force T . (C) Beam's profiles extracted by image analysis from top views during a sequence of motor displacements. Each profile is fitted by a law such that $C(x) = C_{\text{bending}} + C_{\text{shear}}(1 - (x/L))$, where C_{bending} and C_{shear} are fitting parameters and x is the coordinate along the beam. (D) Curvatures measured from the beam profiles as function of the displacement of the motor where $\bar{C} = C_{\text{bending}} + (C_{\text{shear}}/2)$.



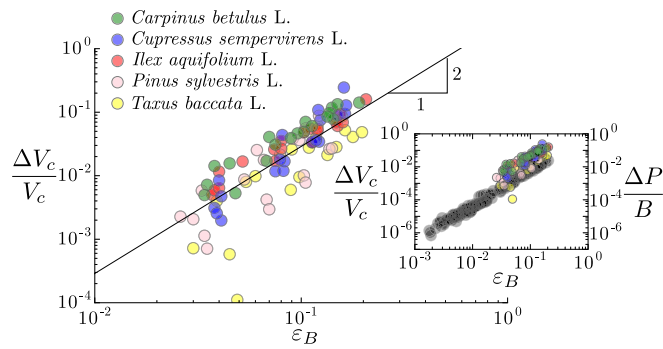
249
250
251
252
253
254
255
256
257
258
259
260
261
262
263 **Fig. S2.** Pressure response to bending normalized by the elastic bulk modulus of the biomimetic branches as function of the bending deformation $\varepsilon_B = \overline{C}R$
264 for a uniform curvature (blue symbols, quadratic fit $y = 0.62x^2$) and a linear variation of curvature (red symbols, quadratic fit $y = 0.97x^2$) (synthetic beams).
265 *Insets* give the measured distribution of curvature along the beams normalized by the beam's length L in both cases.



266
267
268
269
270
271
272
273
274
275
276
277
278
279 **Fig. S3.** Illustration of flattening of an initially curved beam induced by bending.



280
281
282
283
284
285
286
287
288
289
290
291
292
293 **Fig. S4.** Measurement of the channel bulk modulus in poplar branches (*P. alba* × *tremula* L.). (A) Experimental setup used to determine the macroscopic
294 bulk modulus B_{macro} from the relationship between the pressure increments ΔP and the relative change of the branch's volume $\Delta V/V$ (see plot, here
295 $B_{\text{macro}} = 1 \pm 0.02$ GPa). (B) Cytological cross-section for measurement of the channel's fraction ψ (in black) and estimation of B via the relation $B = \psi B_{\text{macro}}$.



Q:4 Fig. 55. Normalized expelled volume of water as function of the bending deformation (the maximal deformation at the center of the branch in a four-point bending setup) on five tree species [computed from the raw data of Lopez et al., 2014 (23)]. The best quadratic fit of the data gives $\Delta V_c / V_c = (2.90 \pm 0.25) \times \varepsilon_B^2$ ($R^2 = 0.68$).

PNAS proof
Embargoed

AUTHOR QUERIES

AUTHOR PLEASE ANSWER ALL QUERIES

Q: 1_Please clarify what is meant by “red inset,” as the figure does not appear to have any Insets. Should it be “red line” or “red squares” instead?

Q: 2_In the Fig. S2 legend, please clarify what is meant by “Insets,” as the figure does not appear to have any Insets. Should it instead be either “solid lines” or “filled squares”?

Q: 3_Please confirm that INRA was spelled out correctly.

Q: 4_In the Fig. S5 legend, please confirm the citation of ref. 23 for Lopez et al. and that it should be 2014 rather than 2016.
